

On the interaction of low molecular weight poly(diallyldimethylammonium chloride) and sodium dodecylsulphate in low surfactant-polyelectrolyte ratio, salt-free solutions

Leesa Patel¹, Omar Mansour², Hannah Bryant¹, Wasiu Abdullahi¹, Robert M. Dalgliesh³ and Peter C. Griffiths^{1,*}

Abstract

Coacervation is widely used in formulations to induce a beneficial character to the formulation but non-equilibrium effects are often manifest. Electrophoretic (eNMR), pulsed-gradient spin-echo NMR (PGSE-NMR) and small-angle neutron scattering (SANS) have been used to quantify the interaction between low molecular cationic poly(diallyldimethylammonium chloride) (PDADMAC) and the anionic surfactant sodium dodecylsulphate (SDS) in aqueous solution as a model for the precursor state to such non-equilibrium processes. The NMR data show that within the low surfactant concentration one-phase region, an increasing surfactant concentration leads to a reduction in the charge on the polymer and a collapse of its solution conformation, attaining minimum values coincident with the macroscopic phase separation boundary. Interpretation of the scattering data reveals how the rod-like polymer changes over the same surfactant concentration window, with no discernible fingerprint of micellar type aggregates, rather the emergence of disc-like and lamellar structures. At the highest surfactant concentration, the emergence of a weak Bragg peak in both the polymer and surfactant scattering suggest these pre-cursor disc and lamellar structures evolve into paracrystalline stacks which ultimately phase separate. Addition of the non-ionic surfactant hexa(ethylene oxide) dodecyl ether (C₁₂E₆) to the system seems to have little effect on the PDADMAC/SDS interaction as determined by NMR, merely displacing the observed behaviour to lower SDS concentrations, commensurate with the total SDS present in the system. In other words, the PDADMAC causes the disruption of the mixed SDS/C₁₂E₆

¹ School of Science, Faculty of Engineering and Science, University of Greenwich, ME4 4TB, UK

² Faculty of Health and Life Sciences, Leicester School of Pharmacy, De Montfort University, The Gateway, Leicester, LE1 9BH, UK

³ ISIS Neutron and Muon Source, Science and Technology Facilities Council, Rutherford Appleton Laboratory, Rutherford Appleton Laboratory, Didcot, Oxfordshire OX11 0QX, UK

micelle, leading to SDS-rich PDADAMC/surfactant complexes coexisting with $C_{12}E_6$ – rich micelles in solution.

Introduction

It is well-known that in the presence of an anionic surfactant, solutions of a cationic polyelectrolyte often show associative phase separation leading to a complex coacervate (concentrated phase) coexisting with a more dilute phase [1-4]. Accompanying such phase separation, is the formation of nanostructures with different morphologies and organisation, including soluble complexes, precipitates, gels and liquid crystalline phases [5,6]. Complex coacervation is further complicated by the presence of interfaces [7-10], but the continued focus on studying coacervation is driven by its relevance to many and diverse applications of formulated, nanostructured systems [11-17].

Coacervation occurs as the result of a complex balance of electrostatic and hydrophobic factors, and therefore depends intimately on the character of the constituent materials, in particular, their concentration, molecular weight, charge density and hydrophobicity, with this balance being mediated by the prevailing solvent conditions, such as temperature, pH and ionic strength [18,19].

Coacervation is however difficult to study, as the underlying phase behaviour shows such a significant dependence on composition which *inter alia* defines or restricts experimental approaches and protocols, compounded by the fact that the phase behaviour often evolves with time [20-25]. Indeed, kinetically trapped structures are frequently evident (and desirable in some applications), both in solution and at interfaces, dependent on sample preparation protocols [26,27].

Notwithstanding these challenges, consensus points to the importance of the ratio of the charges borne by the constituent components - usually expressed in terms of the polyelectrolyte/surfactant ratio – given that the macroscopic phase separation boundary is near-coincident with the point of net zero charge [*e.g.* 1,28-33]. However, most studies in the literature focus on high molecular weight polyelectrolytes due to their useful rheological and (de)stabilising character, or inherently at concentrations away from their useful range [7]. Here, we present a study of a low molecular weight sample of the commonly studied

polyelectrolyte poly(diallyldimethylammonium chloride) (PDADMAC) and its interaction with sodium dodecylsulphate (SDS) in aqueous solution, using NMR methodologies to probe within technologically relevant concentrated solutions, the conformation and charge, and small-angle neutron scattering to probe the state of surfactant aggregation. It was hypothesised that the use of the low molecular weight sample will allow the characterisation of pre-cursor states that give rise to similar structures observed in higher molecular weight species, whilst reducing the impact of any non-equilibrium effects.

Materials and Methods

Materials

Low molecular weight poly(diallyldimethylammonium chloride) (PDADMAC), supplied as a 35wt% aqueous solution by Sigma-Aldrich, was used as received. Analytical grade surfactants sodium dodecylsulphate (SDS) and hexa(ethylene glycol) monododecyl ether (C₁₂E₆) were also supplied by Sigma-Aldrich. Both surfactants were used as received as the surface tension derived critical micelle concentrations and mass spectrometry data showed the absence of impurities, and were consistent with expected structures and literature values.

Methods

The phase boundaries were determined by adding prediluted surfactant stock solutions to polymer stock solutions on a 2g scale in 5ml cylindrical glass vials, shaking end-over-end for 15 sec and then allowing to stand for 1 hr before noting the appearance of the sample. The instability and therefore the macroscopic separation phase boundary was identified as those samples that showed visible heterogeneity. Opaque but otherwise homogeneous samples that did not further change appearance over a longer time period (24hr) were deemed stable, though the opacity clearly indicated the presence of large structures.

The surface tension measurements of the polymer and surfactant solutions were recorded using a maximum bubble pressure tensiometer (SITA t60) that was calibrated with pure water and checked for linearity using water/alcohol mixtures. Measurements were performed in bubble lifetime mode, with the limiting surface tension recorded at long bubble lifetime value, typically longer than 5s. All samples were equilibrated at 25 (\pm 0.5) °C *in situ* using a

recirculating water jacket prior to measurement, and within 24 hours of preparation of the sample.

NMR experiments were carried out at $25 (\pm 0.5) ^\circ\text{C}$ on a 400 MHz Bruker FT NMR spectrometer. In the PGSE-NMR experiment, a stimulated echo sequence was used, in which the diffusion time (Δ) was set to 300 ms, the duration of the gradient pulses (δ) was held constant at 1 ms and their intensity (G) varied from 0.05 - 100 T m^{-1} . Typically, 16-64 scans were accumulated over 32 gradient steps. Self-diffusion coefficients were extracted by fitting the entire dataset *via* CORE modelling based on a specific number of components as described in the text [34]. The voltage - gradient relationship is calibrated using a 1% H_2O in D_2O standard sample and stored in the instrument configuration tables.

For the electrophoretic NMR experiment [35], a double stimulated echo sequence was used with constant field gradient parameters, sufficient to partially attenuate the residual water peak, $\delta = 1 \text{ ms}$, $\Delta = 300 \text{ ms}$, $G = 0.25 \text{ T m}^{-1}$. In this experiment, the electric field is generated (PL Scientific, Stockholm) by applying 0 - 200 V across two blackened platinum electrodes touching the solution at the top and bottom of the sample. The electrodes were prepared by cleaning platinum wire with hydrochloric acid, plated using standard platinising protocols, washed with water, dried and mounted in the eNMR holder using plastic shrink wrap tubing. The electric field, electrode cross-section and separation were calibrated by reference to a known standard – 10 mM tetramethylammonium bromide, $\mu^{\text{TMA}^+} = 3.45 \times 10^{-8} \text{ m}^{-1}$ – such that the slope of the (experimentally determined) phase shift *vs* voltage plot for the sample is simply multiplied by a constant derived from the equivalent TMA^+ dataset to yield the sample electrophoretic mobility. In both cases, calibrations associated with a given probe head (G) and electrophoretic sample environment (electrode area and separation) were determined by (regular) characterisation of the above standards and built into analytical routines.

Small-angle neutron scattering (SANS) experiments were performed on the Larmor diffractometer at the ISIS Spallation Neutron Source, Rutherford Appleton Laboratory, Didcot, UK. A momentum transfer range defined by $Q = (4\pi/\lambda) \sin(\theta/2)$ between 0.0035 and 0.7 \AA^{-1} was obtained by using neutron wavelengths (λ) spanning from 0.9 to 13.5 \AA . The samples were contained in either 1- or 2-mm path length, UV-spectrophotometer grade, quartz cuvettes (Hellma, Germany and Starna Scientific, UK) and mounted in aluminium holders on top of an enclosed, computer-controlled, sample chamber. All experiments were

conducted at 25°C. Experimental measuring times were approximately 60 min. All scattering data were (a) normalized for the sample transmission, (b) background corrected using a quartz cell filled with D₂O, and (c) corrected for the linearity and efficiency of the detector response using the instrument specific software distributed as part of the Mantid framework [36]. SANS experiments were carried out on two series of samples - one with protiated surfactant (scattering length density, $\rho_{h-SDS} = -0.4 \times 10^{-8} \text{ \AA}^{-2}$), one with deuterated surfactant (scattering length density, $\rho_{d-SDS} = 6.8 \times 10^{-8} \text{ \AA}^{-2}$) – both with deuterated solvent, D₂O (scattering length density, $\rho_{D_2O} = 6.4 \times 10^{-8} \text{ \AA}^{-2}$). The (anhydrous) polymer has a calculated scattering length density of (scattering length density, $\rho_{poly} = 0.5 \times 10^{-8} \text{ \AA}^{-2}$). All data were analysed within the SASView package using standard and user-written functions.

Results and Discussion

The stiff character of polyelectrolytes presents a number of the challenges in their study by NMR, typically displaying broad and weak signals associated with a low fraction of mobile regions within the polymer *e.g.* [37]. Nonetheless, pulsed-gradient spin-echo and electrophoretic NMR have been deployed to characterise the mobility of low molecular weight PDADMAC species in the absence of an applied electric field (diffusion, figure 1(a)) and in its presence (electrophoresis, figure 1(b)), and the charge on the polymer *via* the normalised ratio of these two measures of mobility (figure 1(c)) [38]. Both the self-diffusion coefficient and the electrophoretic mobility show a decrease with increasing polymer concentration, although with slightly different functional forms, especially at very low concentrations. An extrapolation to infinite dilution of the diffusion data assuming a power law dependence of the friction opposing that diffusion [19,39], leads an effective hydrodynamic radius of $R_h = 1.0 (+/- 0.2) \text{ nm}$ *via* the Stokes-Einstein equation, assuming an equivalent spherical shape. The magnitude of the size is closer to $R_h = 4.6 (+/- 0.2) \text{ nm}$ for the self-diffusion coefficient measured at a polymer concentration of 1wt%.

The electrophoretic mobilities determined here by NMR are consistent with those for PDADMAC determined by light scattering methods *e.g.* [40,41] albeit at higher molecular weight, as well as with other highly charged oligo- or polymeric structures such as poly(ethylene imine) (PEI) [38] and polyamidoamine (PAMAM) dendrimers [42].

The charge (z) on the species is calculated from the ratio of the electrophoretic mobility (μ) and the self-diffusion coefficient (D_s) normalised for Boltzmann's constant (k_B) and the temperature (T);

$$z = \frac{\mu k_B T}{D_s e} \quad (1)$$

It may be seen that z attains a constant value above a polymer concentration of $C_{PDADMAC} = 1$ wt%. The magnitude of the limiting charge – $2e$ per polymer – seems intuitively low given the nominally highly charged nature of the polymer, which in turn implies a high degree of counterion binding. Such counterion binding under the experimental conditions here - the NMR timescale (300 ms) and salt-free solutions - is consistent with both the NMR [37] and dielectric spectroscopy analyses [43] of the PDADMAC chain which centres on modelling two populations of counterions – one tightly bound population leading to the mobile sections of the polyelectrolyte, and a second loosely bound population diffusing parallel and perpendicular to the PDADMAC chain. We shall return to this discussion of the charge after the presentation of the SANS data.

Mixtures of oppositely charged polymer and surfactants usually show regions of macroscopic phase separation coincident with pronounced “steps” in the surface tension data [*e.g.* 44], in marked contrast with the behaviour observed for non-ionic polymer and charged surfactant systems [*e.g.* 45], the latter showing no such “steps” in the surface tension data, merely transitions into- and out- of plateau-like regions. Over this low-surfactant concentration, one-phase region, it is usually assumed that the surfactant binds molecularly to the oppositely charge groups on the polymer, leading to a neutralisation of the polymer/surfactant complex.

The phase behaviour - figures 2(a) and 2(b) - and surface tension data – figure 2(c) - for the binary PDADMAC/SDS mixtures studied here show this expected behaviour. Figures 2(b) and 2(c) presents the various datasets on a normalised concentration scale, intended to be a simple representation of the anionic/cationic charge ratio over the experimental window. Over the entire range of PDADMAC concentration studied $0.25 < C_{PDADMAC} < 1$ wt%, the phase boundary occurs at $C_{SDS}/C_{PDADMAC} = 40 (\pm 10)$ for the phase behaviour and

$C_{SDS}/C_{PDADMAC} = 50 (\pm 5)$ for the surface tension behaviour. The fact that both experimental methodologies collapse onto a similar ratio confirms the origin of the features in the data are

dominated by charge neutralization. It will be shown later that this concentration ratio corresponds to a charge ratio of unity.

Our focus is therefore limited to the low SDS one-phase concentration window, *viz* for 1wt% PDADMAC solution, $0 < [\text{SDS}] < 40 \text{ mM}$, with samples at the higher end of these SDS concentrations being milky but stable. Above $C_{\text{SDS}} = 40 \text{ mM}$, the samples phase separate, but re-dissolve for $C_{\text{SDS}} > 50 \text{ mM}$.

The peaks in the PDADMAC NMR spectra overlap with the SDS and therefore, the peaks in the 2-4 ppm range will contain contributions from both species. Notably, the SDS signal is quite weak (compared to its no-polymer comparator), indicating that the SDS is in a rather motionally restricted environment, and its relaxation is efficient (data not presented) [27]. A careful analysis of the spectra in conjunction with parallel measurements on selected samples using deuterated SDS (to remove any signal from the surfactant), indicated that both the decay of all signal intensities (diffusion) and the phase shifts (electrophoresis) could be appropriately analysed by a *single component*, indicating that both the polymer and the surfactant exhibit the same self-diffusion coefficient and electrophoretic mobilities. One concludes therefore, that the unimer (non-polymer-bound) surfactant concentration is low, a conclusion that is reinforced by the coincidence of the phase boundary and surface tension data in figures 2(b) and 2(c).

The derived self-diffusion coefficients, electrophoretic mobilities and charges on the polymer/surfactant complex are presented in figures 3(a,b,c). With increasing SDS concentration, the self-diffusion coefficient of the polymer *increases* indicating a contraction in the conformation of the polymer, presumably associated with the reduction in the electrostatic repulsion between the charged moieties along the polymer backbone. Consistent with that hypothesis is the fact that the electrophoretic mobility decreases with increasing SDS concentration, indicating a decreasing cationic charge on the complex. Not surprisingly, the binding of the anionic surfactant to the cationic polymer results in a reduction in the charge on the complex, figure 3(c), reaching a zero value coincident with the macroscopic phase separation boundary and the “step” in the surface tension data.

The structure of the PDADMAC/SDS complex has been explored by small-angle neutron scattering across this low surfactant concentration, one phase region of the phase diagram.

The measured small-angle neutron scattering data are presented in figures 4(a) and 4(b) for these two series of samples. Consider initially, the gross features in the data, which are consistent with other such studies [15,29,46,47]. Firstly, note (a) that the scattering from the polymer alone is very weak, consistent with a small highly hydrated solution confirmation, and (b) the very broad peak in that scattering over the mid-Q range, a feature that is reminiscent of surfactant scattering, consistent with a moderate concentration of small, charged scatterers. The form of the data – a broad peak - is also similar to that observed for larger molecular weight polyelectrolytes. Secondly, the general appearance of the two sets of experiments (figures 4(a) vs 4(b)) are remarkably similar, indicating that the size and/or distribution of the polymer and the surfactant *within* the polymer/surfactant complex are both *mutually* similar, *and* similar to the overall size & shape of the complex. Note there is significantly more intensity when the protiated surfactant is used, a point that we shall return to below. Thirdly, the most notable change in these “paired” datasets induced by the addition of the surfactant, is the increase in scattering intensity at low Q, which may arise due to the presence of larger or differently-shaped structures and/or a transition from repulsive interparticle interactions into attractive ones. As is evident from the limiting slopes indicated in figure 4(a), the functional form of these with-surfactant datasets at low Q increases from Q^{-1} (characteristic of rod-like structures) through Q^{-2} (which, depending on the size of the structures, may be indicate the presence of curvature *e.g.* surfactant aggregates, or flatter structures, such as discs) into Q^{-4} for the highest surfactant concentration sample consistent with large, homogeneous scatterers (though such a definitive identification of the likely shape requires an absence of an $S(Q)$ term). Finally, there is a clear appearance of an inflection or a bump in the data over the mid-Q range, and at the highest surfactant concentration a noticeable Bragg peak at $Q = 0.167 \text{ \AA}^{-1}$, consistent with a dimension of 38 \AA . This dimension is similar in magnitude to twice the length of an SDS molecule, implying the existence of lamellar type structures.

Consider first just the simple polymer solution. Merta *et al* [48] interpreted scattering from PDADMAC with molecular weight 300K g mol^{-1} in terms of two models based on a cylinder morphology, obtaining values for the cross-section of $5 (\pm 2)$ and $16 (\pm 1) \text{ \AA}$, though the simpler model under-represented the weak peak in the data. In a similar vein, the scattering from the 1wt% low molecular weight PDADMAC solution here was also well-described by a surfactant-inspired cylindrical morphology invoking a rod-like form factor with radius $R = 6 (\pm 0.5) \text{ \AA}$ similar to Merta *et al*, and length $L = 70 (\pm 2) \text{ \AA}$. In contrast to Merta *et al*, here a

Hayter-Penfold structure factor ($S(Q)$) has been included to treat the peak in data, yielding an ionic character commensurate with $5e$ per molecule [49]. Therefore, recalling the previous NMR analyses, all indications point to a small polymer that bears a low charge. In the absence of any definitive molecular weight information, these various analyses may be combined to recalculate an average value for the degree of polymerization (DP), and thereafter, to interpret fully the charge on the polymer. Recalling that in these salt-free solutions, the polymer adopts a rod-like conformation with $L = 7.0$ nm, this corresponds to an equivalent-spherical-volume radius of 1.1 nm, in good agreement with the extrapolated infinite-dilution hydrodynamic radius of $R_h = 1.0$ (+/- 0.2) nm from the NMR data. The experimental data are therefore in excellent mutual agreement. Adopting the Kuhn statistical length for the monomer unit (0.54 nm) employed by Chen *et al* [43], indicates that this rod length is consistent with $DP \approx 13$, or molecular weight $M_w \approx 2,100$ g mol⁻¹. Thus, the charge of $2e$ per molecule from the eNMR data suggests a degree of counterion dissociation of 15%. The SANS data are however, equally well-described by an unscreened polyelectrolyte “broad peak” model [50] with the same system parameters (molecular weight, scattering length densities, concentration and monomer length) derived in this iterative NMR/SANS analysis, but allowing the degree of counterion dissociation to increase to 21%.

Continuing this aside, based on this estimate for the molecular weight (and therein effective molecular volume), the polymer *number* concentration may be used to calculate the critical overlap concentration (C^*) and to reframe the charge ratio coincident with the phase behaviour and the surface tension data. C^* for these systems would be $C_{poly} > 10$ wt%, thus negating any correction for obstruction effects in the NMR analyses. More importantly, the *charge* ratio commensurate with the concentration ratio of $C_{SDS}/C_{PDADMAC}$, *i.e.* that delineating the phase boundary from the visual (40 (± 10)) or surface tension (50 (± 5)) analyses corresponds to a charge ratio of 0.95 (± 0.18), in excellent agreement with the literature value of 1.

Returning to the SANS data, consider the detail in figures 4(a) and 4(b). The purpose of such a paired “contrast variation” experiment where two series of samples have been studied – one with protiated surfactant (figure 4(a)) and a second otherwise identical series with deuterated surfactant (figure 4(b)) – is to provide structural information on the internal structure of the complex. Under these conditions, the scattering from the deuterated surfactant in deuterated

solvent is significantly depressed, such that the observed scattering is dominated by the polymer, and where the surfactant is protiated, the scattering arises from both polymer and surfactant. The striking similarity in the shape of the scattering curves of the paired samples indicates that the structure of the *complex* is very similar to the *polymer* one (*i.e.* in the presence of the invisible surfactant), illustrating the strength of “templating” by the polymer.

The intensity of the scattered radiation, $I(Q)$, arising from these polymer / surfactant complexes, as a function of the wavevector, Q , is given by Equation (2):

$$I_i(Q) = N_i V_i^2 (\rho_i - \rho_{solv})^2 P_i(Q) S_i(Q) + B_{inc} \quad (2)$$

where B_{inc} is the incoherent background, N_i is the number and V_i the volume of the scattering species, $(\rho_i - \rho_{solv})$ is the difference between the neutron scattering length density of the scattering species (i) and the solvent ($solv$), $P_i(Q)$ describes the morphology of the scattering species and $S_i(Q)$ their spatial distribution in solution.

A number of standard models often utilised in understanding polymers/surfactant assemblies were tested against the data *via* $P_i(Q)$. These included; Debye and other representations for the polymer; micelles, both spherical and elongated; core-shell structures; lamellar based assemblies, including single and multi-layer vesicles. The majority of these models were found to poorly reproduce the scattering observed at low Q , typically under representing that part of the dataset, *and* often failing to reproduce the subtle features in the data around mid Q . Clearly, length scales over more than one characteristic range must be present. The subtle peaks in the data at mid Q were found to be reasonably well-reproduced by form factors from lamellae and/or stacked discs, although both under represented the intensity at low Q .

Therefore, a composite model has been constructed comprising terms to account for the *local* (lamellae, discs) and *global* structures using the built-in feature of SASView, *viz*;

$$I_{complex}(Q) = aI(Q)^{local} + bI(Q)^{global} \quad (3)$$

with amplitudes a and b respectively collecting all the pre-terms in Eqn (2). The *local* term accounts for the scattering arising from the structure of the molecular polymer/surfactant complex and the *global* term accounts for the assembly of those molecular polymer/surfactant

complexes. For the higher SDS concentration samples, this follows a Q^{-4} commensurate with larger structures that give rise to the slightly milky appearance of the samples.

Informed by a reasoned consideration of possible structures, one arrives at a structure in which the core region principally comprises the surfactant tails, with the polymer and surfactant headgroups residing in an outer, hydrated layer, as illustrated in Figure 5. Thus, initial estimates of the scattering length densities of these regions may be selected, assuming a level of hydration. Ultimately, the models used comprised stacked disks with a Q^{-4} term for the higher SDS concentration samples, and a combined stacked disc / lamellar model at the lowest SDS concentration, without the Q^{-4} term.

As may be seen by the fits in figures 4 (a,b) this approach is a good representation of the data, notwithstanding its complexity. Absolute intensities are consistent with the composition of the sample and its concentration. For SDS concentrations above 5 mM, 10 stacks of discs were invariably included in the analysis. Interestingly, the parameters are relatively consistent across both contrasts and surfactant concentration - the radius (R) of the disc $23.8 (\pm 3.7) \text{ \AA}$ with a combined core + layer thickness of $33.5 (\pm 5.5) \text{ \AA}$. For the protiated surfactant, the core thickness is marginally greater than the deuterated case ($25.0 (\pm 5.1) \text{ \AA}$ vs. $20.3 (\pm 3.1) \text{ \AA}$), though this variance is accommodated in the opposite trend in the layer thickness ($10.0 (\pm 5.9) \text{ \AA}$ vs. $13.0 (\pm 3.5) \text{ \AA}$). This length scale - $33.5 (\pm 5.5) \text{ \AA}$ - is consistent with twice the fully extended length of the dodecyl chain. Financially, it is clear that the Bragg peak is well-reproduced in this modelling.

Complex formulation rarely include just a single surfactant or polymer, non-ionic polymers or surfactants being added to modulate the interaction between the (oppositely) charged species [*e.g.* ^{2,41,51-55}]. Many of these studies focus on higher surfactant concentrations and the non-ionic species induced resolubilisation of the (insoluble) complex formed between the oppositely charged polyelectrolyte and surfactant [*e.g.* ^{54,56}]. A number of mechanisms are hypothesised; the non-ionic species reducing the effective charge on the mixed micelle and therefore suppressing its interaction with the oppositely charged polyelectrolyte, a model that is limited to concentrated surfactant systems [²⁴]; the ionic surfactant is “stripped” from the polyelectrolyte complex reducing the tendency to phase separate [⁵⁷], because it preferentially resides in the mixed micelles; or where the polyelectrolyte/ionic surfactant complex coexists in equilibrium with non-ionic micelles [⁵⁸].

Therefore, to understand further the dominating effect of the electrostatic character of the interaction, a competing non-ionic surfactant – hexaethylene mono dodecyl ether ($C_{12}E_6$) - has been added to the PDADMAC/SDS system to quantify any perturbation to the electrostatic interaction between PDADMAC and SDS. This is akin to the “low ionic surfactant-to-polyion ratio” chemical model proposed by Fegyver and Mészáros [2]. The phase behaviour is presented in figures 6(a) and 6(b), the latter expressed in the normalised surfactant-to-polymer concentration ratio, $C_{SDS}/C_{PDADMAC}$. In these ternary systems, C_{SDS} may be varied both by the total surfactant concentration C_{total} and the solution mole fraction α_{SDS} , viz $C_{SDS} = \alpha_{SDS} C_{total}$.

Addition of the non-ionic pushes the phase separation boundary to higher total surfactant concentrations, figure 6(a), but the effect is considerably weaker when plotted in terms of the $C_{SDS}/C_{PDADMAC}$ ratio, figure 6(b). Interestingly, for these ternary systems $C_{SDS}/C_{PDADMAC} = 40 (\pm 3)$ in striking agreement with the binary case, suggesting that the non-ionic surfactant is merely a “spectator” in the PDADMAC/SDS interaction.

The two NMR techniques were again deployed to study these ternary systems, at $C_{PDADMAC} = 1$ wt%, but in the presence of the two surfactants at a total concentration $C_{total} = 30$ mM and by varying the surfactant mole fraction, *i.e.* still just inside the one-phase region of the phase diagram.

The NMR data / spectra are now increasingly more complex, and more involved approaches must be invoked to analyse the data given the number of components present in the system. In the diffusion experiment, one follows the attenuation of the intensity of one or more peaks. Whilst these decays may sometimes be combined into a single peak, the component decays are independent and therefore separable through model fitting. For systems with $0.3 < \alpha_{SDS} < 0.8$, both two- and three-component fits were tested against the data, but generally the two-component approach was found to be sufficient. Attempts to deconvolute the surfactant spectra into its two components *viz* SDS and $C_{12}E_6$ did not lead to improved fits. It is concluded *from the nature of the analysis*, that the model is best described by a dynamics model that invokes very rich $C_{12}E_6$ micelles coexisting with PDADMAC/SDS complexes. Further, as in the binary case, most (perhaps all) of the SDS is associated with the polymer, and *inter alia* that the SDS spectrum is strongly suppressed due to relaxation time effects. An additional complication arises in that at the extremes of the mole fraction range, $\alpha_{SDS} < 0.3$

and $\alpha_{SDS} > 0.8$, the two limiting cases reduce to one component fits, because for $\alpha_{SDS} > 0.8$, the PDADAMC/SDS complex diffuses as a single entity, and for $\alpha_{SDS} < 0.3$, the PDADMAC and C₁₂E₆ diffuse independently but have the same numerical self-diffusion coefficient, as confirmed in the single component solutions.

In the electrophoresis experiment, one has to determine a phase shift associated with one or more peaks, but these are not independent, and affect the various peaks to a degree based on its mobility. The water peak is usually invoked as the “calibrant”. As an illustration, figure 7 presents three paired spectra, for the case when there is no applied electric field (left column), and therefore no electrophoretic motion, and when an electric field has been applied (right column). For the non-ionic rich systems, *e.g.* top row, the level of phase correction required for the alkyl peak is very small, and comparable to the water peak, but different to the polymer peak as evidenced by the negative tail on the right of the 2-3 ppm peaks; therefore the surfactant (like the water) has a zero average mobility, but the polymer is non-zero. The phase shift of the polymer peak cannot but corrected by the same factor, and thus the polymer is undergoing electrophoretic flow – it is charged. Thus, one may also conclude that since the non-ionic surfactant exhibits little electrophoretic mobility, it is not interacting with the polymer. This is entirely consistent with the diffusion interpretation.

For the anionic-rich systems, *e.g.* bottom row, again a single phase correction seems to correct all the polymer and surfactant peaks equivalently (and to a degree greater than that needed for the water peak). This single correction is consistent with a charged PDADMAC/SDS complex, and a very small contribution to the peak intensity from the (free) C₁₂E₆ (micellar) component.

For mole fractions in the middle of the composition range ($0.3 < \alpha_{SDS} < 0.8$), the situation is rather complex, with no single phase adjustment adequately correcting all the peaks, simultaneously, evidenced in terms of the slight negative intensity around 2.5 – 3.0 ppm, the middle spectra in figure 7. Whilst elegant methods to deconvolute such overlapping spectra in electrophoretic NMR experiments have recently been presented, the spectra here do not lend themselves to that level of scrutiny, and a semi-empirical analysis is presented [59].

Consider first the polymer self-diffusion coefficients in the binary PDADMAC/SDS system and the ternary PDADMAC/SDS/ C₁₂E₆ system, plotting both in terms of the SDS solution

concentration, figure 8(a). As might be expected, the polymer self-diffusion coefficients at the limits of SDS concentration merge, given the ternary system collapses to the binary one in the when $\alpha_{SDS} = 1$, and slight reduction in the polymer diffusion when $\alpha_{SDS} = 0$ i.e. 30mM $C_{12}E_6$ alone, may be understood in terms of a slight obstruction effect due to the surfactant micelle. Over the intermediate range of prevailing SDS concentration, accessible through changes in surfactant concentration directly (binary systems) or surfactant composition, α_{SDS} (ternary systems), a common behaviour is observed, through the polymer does appear to diffuse slightly faster in the ternary solution. Slightly bigger differences are observed in the electrophoretic mobility data, figure 8(b), though note the relative scales. The electrophoretic mobility of the polymer when $\alpha_{SDS} = 0.0$ is comparable to the polymer-only value. Now, the electrophoretic mobility of the polymer in the ternary case is greater (more positive) than in the binary case, over the majority of the SDS concentration range, suggesting that there is less SDS bound to the polymer (to neutralise some of the cationic charge), as found by Fegyver and Mészáros [2] in their study on PDADMAC/SDS/dodecyl maltoside ($C_{12}G_2$) system.

The charge on the polymer/surfactant complex in the binary and ternary systems is presented in figure 8(c), and a remarkable similarity is observed between the two systems. There are subtle differences in the data at low SDS concentrations. Over this region at least, the data suggest that $C_{12}E_6$ may be perturbing the binding of the SDS to the PDADMAC (electrophoretic mobility) but seemingly not significantly affecting its solution conformation (diffusion). However, for these non-negligible concentrations, the effects of obstruction cannot be unequivocally removed. The universality of these NMR data, plotted in this fashion, and the coincidence of the phase behaviour, does however lend considerable support to a model in which the SDS binds almost stoichiometrically to the PDADMAC, neutralising the charge, and that the $C_{12}E_6$ has an insignificant impact on the PDADMAC/SDS interaction. This behaviour embodies characteristics of the “stripping” formalism at low α_{SDS} [57] and a re-equilibration mode at higher α_{SDS} [58].

As a predominantly electrostatic interaction, the proximity of the various charge groups is central to defining the interaction. Surfactant headgroup - monomer charge neutralisation leads to changes in the polymer conformation due to the reduced electrostatic interactions along the backbone, moderated by the formation of local structures necessary to shield the hydrophobic moieties from the aqueous phase. Here, the selection of the low molecular weight polymer precludes any larger length-scale rearrangements of the polymer, and it is hypothesised that only the local structure is accessible here. One can draw an analogy with the blob or scaling theories that define semi-dilute polymer conformations. Closer proximity of opposite charges may be facilitated by increasing the ionic strength, which may independently have significant impacts on polymer conformation as well as the morphology of the aggregated state. The relevance of the simplification of studying a low molecular weight polymer sample as here will require future validation.

Conclusions

Electrophoretic- (eNMR) and pulsed-gradient spin-echo NMR (PGSE-NMR), in conjunction with small-angle neutron scattering (SANS) have been used to quantify the impact of the anionic surfactant sodium dodecylsulphate (SDS) on low-molecular weight, highly-charged poly(diallyldimethylammonium chloride) (PDADMAC) in aqueous solution within the low surfactant concentration one-phase region of the phase diagram. It is shown that binding of the surfactant drives a transition from the highly charged, rod-like polymer-only conformation into ordered layer structures exhibiting lower charge, with evidence of the emerging character of a lamellar structures just prior to phase separation. On addition of a competing non-ionic surfactant, hexa(ethylene glycol) monododecyl ether ($C_{12}E_6$), it is argued that the dominating electrostatic interaction between the PDADMAC and SDS, causes the disruption of the mixed SDS/ $C_{12}E_6$ micelle, leading to PDADMAC/SDS complexes coexisting with non-ionic-rich micelles in solution.

Acknowledgements

The University of Greenwich is acknowledged for the provision of a part-scholarship (WA) whilst the Science and Technologies Research Council is thanked for the provisional of neutron beamtime.

Figures

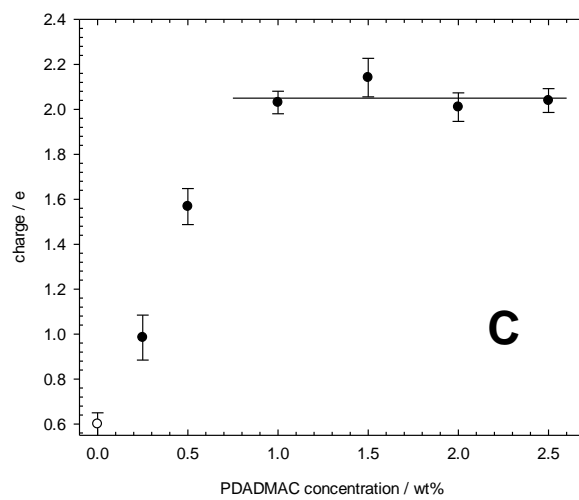
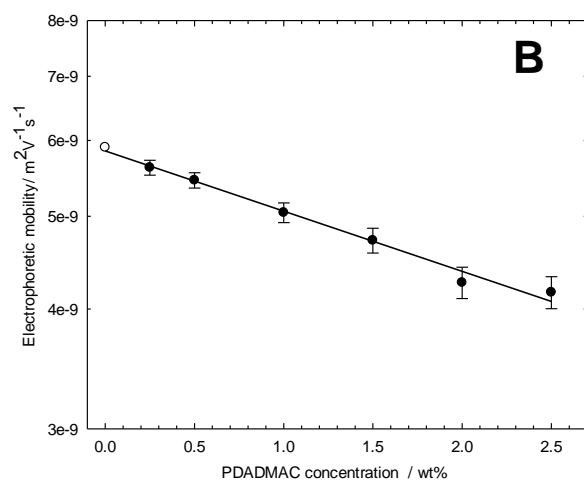
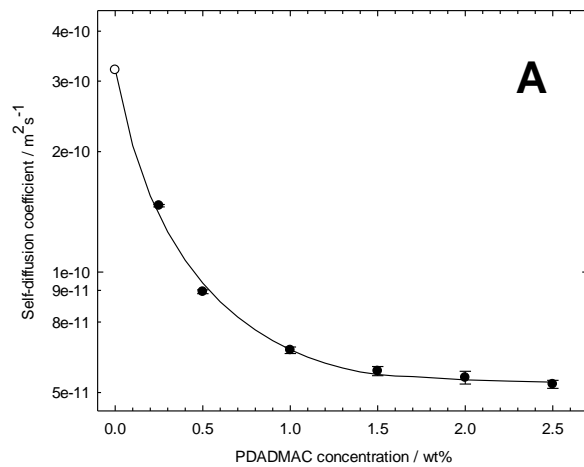
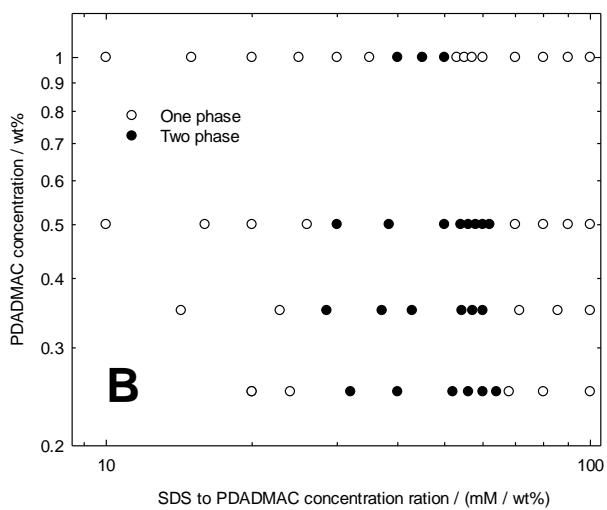
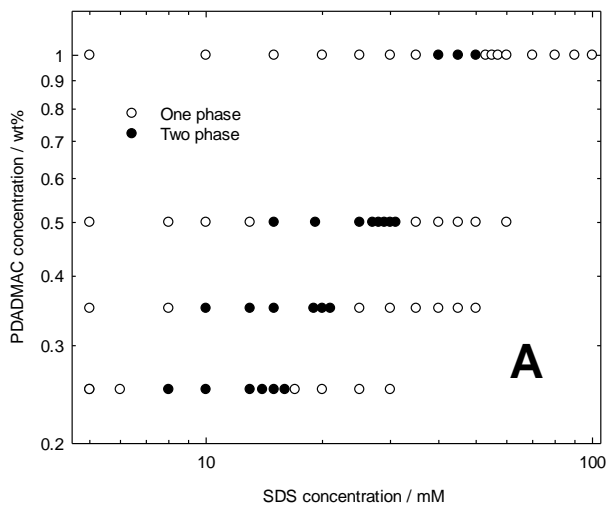


Figure 1 - Diffusion coefficients (a), electrophoretic mobilities (b) and the effective charge (c) of PDADMAC in aqueous solution as a function of polymer concentration, in D₂O at 25 °C. The two sets of data have been interpolated – for the diffusion data, a second order polynomial friction analysis has been used as per [19,39], whereas only a linear relationship is necessary for the electrophoretic data.



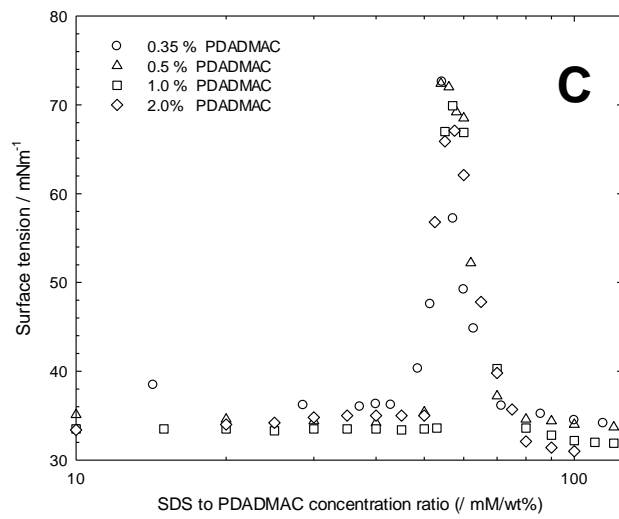
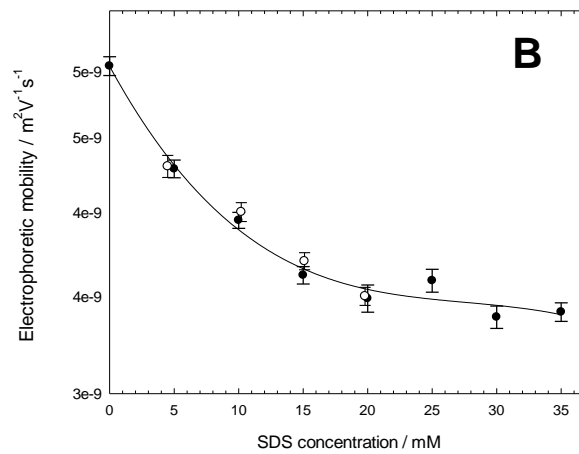
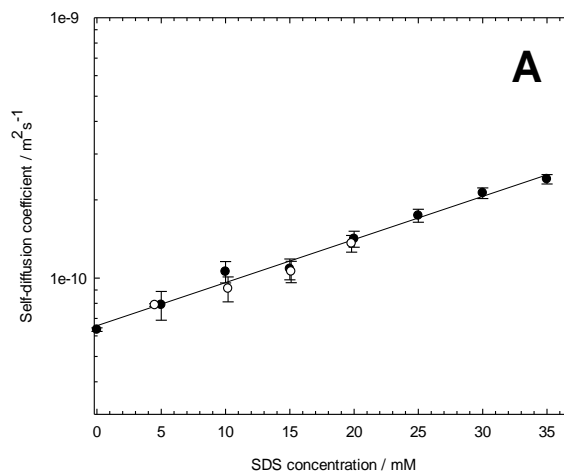


Figure 2 - Phase behaviour (a), and the same phase behaviour (b) and surface tension (c) normalised to the surfactant/polymer concentration ratio for binary mixtures of PDADMAC/SDS, in H_2O at $25\text{ }^\circ\text{C}$.



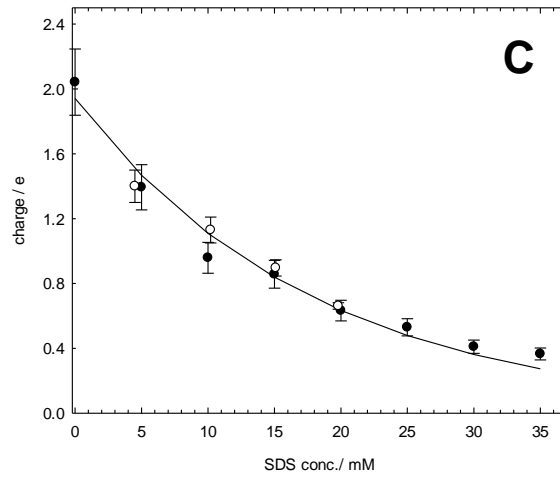
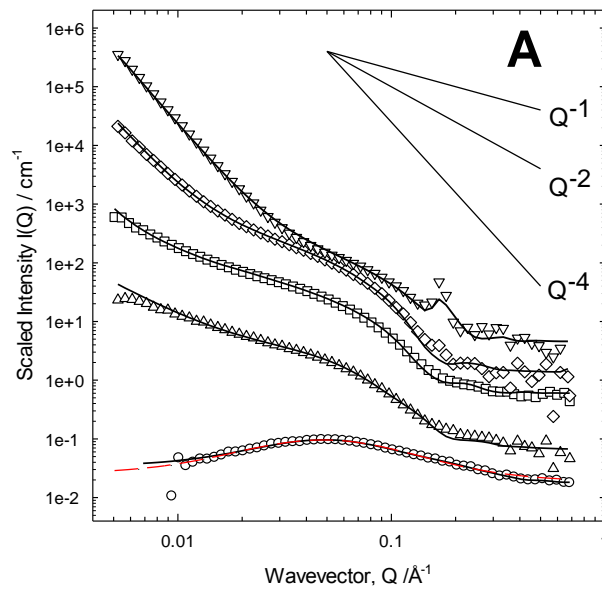


Figure 3 - Self-diffusion coefficient (a), electrophoretic mobility (b) and effective charge (c) of PDADMAC/SDS complexes as a function of SDS concentration, in D_2O at 25 °C with 1wt% PDADMAC. Filled symbols protiated SDS, empty deuterated SDS. Lines are added merely as guides to the eye.



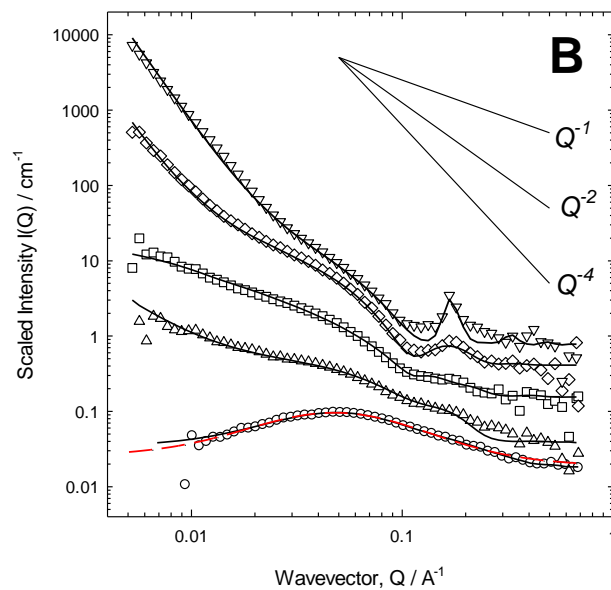


Figure 4 – Scaled small-angle neutron scattering from binary mixtures of PDADMAC/SDS with deuterated (a) and protiated (b) SDS as a function of SDS concentration with 1wt% PDADMAC. Each dataset is offset by $\times 5$ from the previous. Symbols – open circles no SDS; open triangles up 5mM SDS; open squares 10mM; open diamonds 20mM SDS and open triangles down 30mM SDS. The solid lines in figure 4(a/b) correspond to the fits described in the text. The solid inset lines in figure 4(a/b) illustrate Q^{-1} , Q^{-2} and Q^{-4} behaviours.

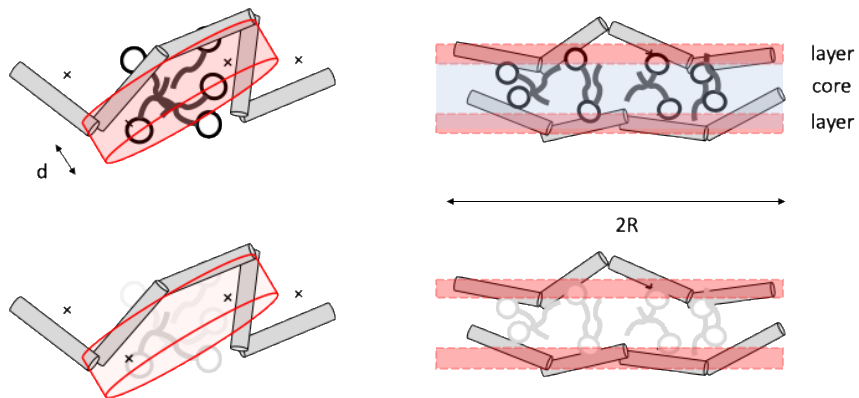


Figure 5; Representations of the model(s) invoked here in the analysis of the SANS data from aqueous PDADMAC/SDS solutions; protiated (top) and deuterated surfactant (bottom).

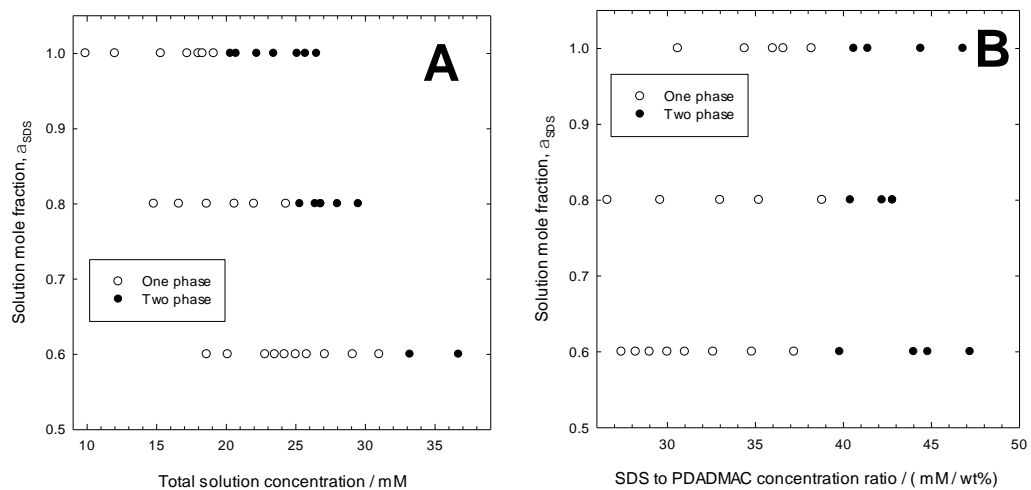


Figure 6 - Phase behaviour for ternary mixtures of 0.5wt% PDADMAC/ $C_{12}E_6$ /SDS as a function of (a) the total surfactant solution concentration and (b) the SDS solution concentration

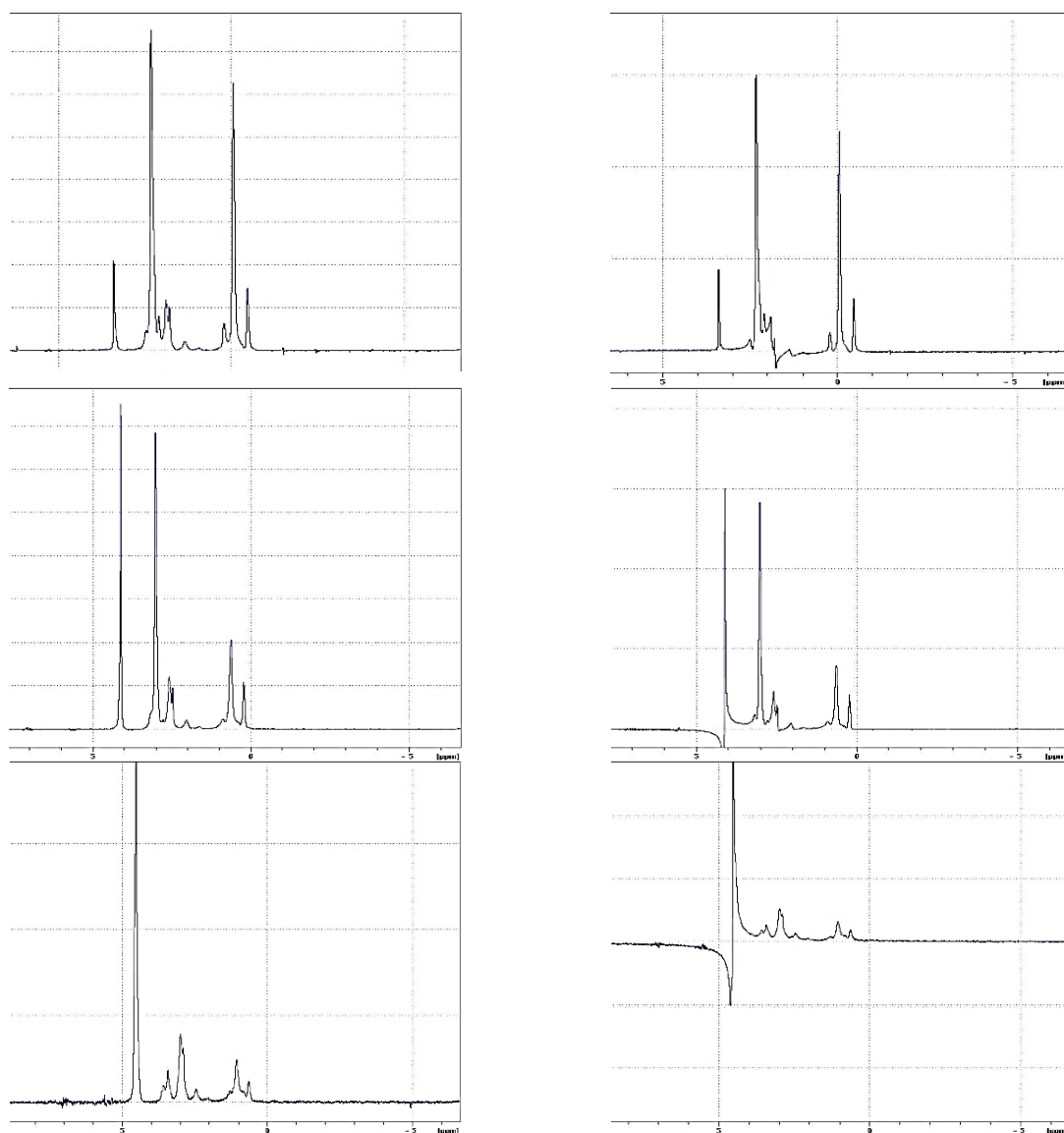


Figure 7 - NMR spectra extracted from the eNMR dataset (left column, no field; right column, voltage applied, 200 V) of PDADMAC/SDS/C₁₂E₆ solutions with $\alpha_{\text{SDS}} = 0.0$ (top row), 0.4 (middle row) and 0.90 (bottom row), all in D₂O at 25 °C.

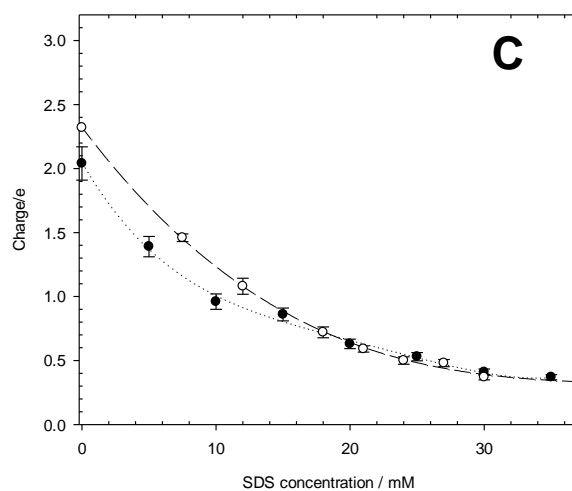
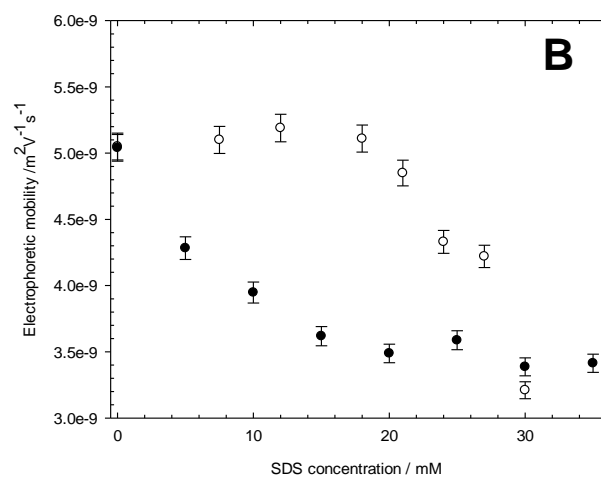
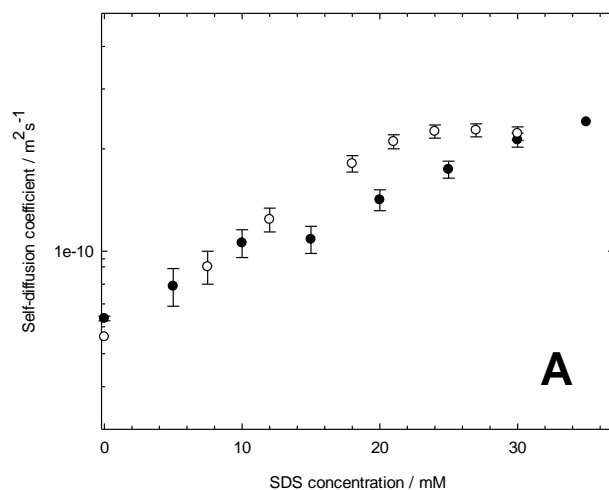


Figure 8 - Self-diffusion coefficients (a), electrophoretic mobilities (b) and effective charge (c) of PDADMAC in the binary PDADMAC/SDS (filled symbols) and ternary PDADMAC/SDS/C₁₂E₆ (empty symbols) mixtures as a function of total SDS present, with 1wt% PDADMAC in D₂O at 25 °C. For the ternary mixtures, C_{SDS} is given by C_{surfactant} α_{SDS}.

References

- (1) Li, D.; Kelkar, M. S.; Wagner, N. J. Phase Behavior and Molecular Thermodynamics of Coacervation in Oppositely Charged Polyelectrolyte/Surfactant Systems: A Cationic Polymer JR 400 and Anionic Surfactant SDS Mixture. *Langmuir* **2012**. <https://doi.org/10.1021/la301475s>.
- (2) Fegyver, E.; Mészáros, R. Fine-Tuning the Nonequilibrium Behavior of Oppositely Charged Macromolecule/Surfactant Mixtures via the Addition of Nonionic Amphiphiles. *Langmuir* **2014**. <https://doi.org/10.1021/la503928x>.
- (3) Kogej, K. Association and Structure Formation in Oppositely Charged Polyelectrolyte-Surfactant Mixtures. *Advances in Colloid and Interface Science*. 2010. <https://doi.org/10.1016/j.cis.2009.04.003>.
- (4) Sing, C. E. Development of the Modern Theory of Polymeric Complex Coacervation. *Advances in Colloid and Interface Science*. Elsevier B.V. January 1, 2017, pp 2–16. <https://doi.org/10.1016/j.cis.2016.04.004>.
- (5) Xu, A. Y.; Kizilay, E.; Madro, S. P.; Vadenais, J. Z.; McDonald, K. W.; Dubin, P. L. Dilution Induced Coacervation in Polyelectrolyte-Micelle and Polyelectrolyte-Protein Systems. *Soft Matter* **2018**. <https://doi.org/10.1039/c7sm02293j>.
- (6) Kizilay, E.; MacCarrone, S.; Foun, E.; Dinsmore, A. D.; Dubin, P. L. Cluster Formation in Polyelectrolyte - Micelle Complex Coacervation. *J. Phys. Chem. B* **2011**. <https://doi.org/10.1021/jp109788r>.
- (7) Llamas, S.; Fernández-Peña, L.; Akanno, A.; Guzmán, E.; Ortega, V.; Ortega, F.; Csaky, A. G.; Campbell, R. A.; Rubio, R. G. Towards Understanding the Behavior of Polyelectrolyte-Surfactant Mixtures at the Water/Vapor Interface Closer to Technologically-Relevant Conditions. *Phys. Chem. Chem. Phys.* **2018**. <https://doi.org/10.1039/c7cp05528e>.
- (8) Varga, I.; Campbell, R. A. General Physical Description of the Behavior of Oppositely Charged Polyelectrolyte/Surfactant Mixtures at the Air/Water Interface. *Langmuir* **2017**,

33 (23), 5915–5924. <https://doi.org/10.1021/acs.langmuir.7b01288>.

- (9) Uhlig, M.; Löhmann, O.; Vargas Ruiz, S.; Varga, I.; Von Klitzing, R.; Campbell, R. A. New Structural Approach to Rationalize the Foam Film Stability of Oppositely Charged Polyelectrolyte/Surfactant Mixtures. *Chem. Commun.* **2020**. <https://doi.org/10.1039/c9cc08470c>.
- (10) Campbell, R. A.; Yanez Arteta, M.; Angus-Smyth, A.; Nylander, T.; Noskov, B. A.; Varga, I. Direct Impact of Nonequilibrium Aggregates on the Structure and Morphology of Pdadmac/SDS Layers at the Air/Water Interface. *Langmuir* **2014**, *30* (29), 8664–8674. <https://doi.org/10.1021/la500621t>.
- (11) Budhathoki, M.; Barnee, S. H. R.; Shiau, B. J.; Harwell, J. H. Improved Oil Recovery by Reducing Surfactant Adsorption with Polyelectrolyte in High Saline Brine. *Colloids Surfaces A Physicochem. Eng. Asp.* **2016**. <https://doi.org/10.1016/j.colsurfa.2016.03.012>.
- (12) Ferreira, G. A.; Loh, W. Liquid Crystalline Nanoparticles Formed by Oppositely Charged Surfactant-Polyelectrolyte Complexes. *Current Opinion in Colloid and Interface Science*. 2017. <https://doi.org/10.1016/j.cocis.2017.08.003>.
- (13) Lencina, M. M. S.; Fernández Miconi, E.; Fernández Leyes, M. D.; Domínguez, C.; Cuenca, E.; Ritacco, H. A. Effect of Surfactant Concentration on the Responsiveness of a Thermoresponsive Copolymer/Surfactant Mixture with Potential Application on “Smart” Foams Formulations. *J. Colloid Interface Sci.* **2018**. <https://doi.org/10.1016/j.jcis.2017.10.090>.
- (14) Duan, G.; Haase, M. F.; Stebe, K. J.; Lee, D. One-Step Generation of Salt-Responsive Polyelectrolyte Microcapsules via Surfactant-Organized Nanoscale Interfacial Complexation in Emulsions (SO NICE). *Langmuir* **2018**. <https://doi.org/10.1021/acs.langmuir.7b01526>.
- (15) Simon, M.; Krause, P.; Chiappisi, L.; Noirez, L.; Gradzielski, M. Structural Control of Polyelectrolyte/Microemulsion Droplet Complexes (PEMECs) with Different Polyacrylates. *Chem. Sci.* **2019**, *10* (2), 385–397. <https://doi.org/10.1039/C8SC04013C>.

- (16) Gruber, J. V. PolyQuaternium-10: Cornerstone of a Personal Care Revolution. *J. Cosmet. Sci.* **2009**, *60*, 385–386.
- (17) Schmitt, C.; Turgeon, S. L. Protein/Polysaccharide Complexes and Coacervates in Food Systems. *Advances in Colloid and Interface Science.* 2011. <https://doi.org/10.1016/j.cis.2010.10.001>.
- (18) Gradzielski, M.; Hoffmann, I. Polyelectrolyte-Surfactant Complexes (PESCs) Composed of Oppositely Charged Components. *Current Opinion in Colloid and Interface Science.* 2018. <https://doi.org/10.1016/j.cocis.2018.01.017>.
- (19) Patel, L.; Mansour, O.; Crossman, M.; Griffiths, P. Electrophoretic NMR Characterization of Charged Side Chain Cationic Polyelectrolytes and Their Interaction with the Anionic Surfactant, Sodium Dodecyl Sulfate. *Langmuir* **2019**, *35* (28). <https://doi.org/10.1021/acs.langmuir.9b01324>.
- (20) Bali, K.; Varga, Z.; Kardos, A.; Mészáros, R. Impact of Local Inhomogeneities on the Complexation between Poly(Diallyldimethylammoniumchloride) and Sodium Dodecyl Sulfate. *Colloids Surfaces A Physicochem. Eng. Asp.* **2019**. <https://doi.org/10.1016/j.colsurfa.2019.04.052>.
- (21) Naderi, A.; Claesson, P. M.; Bergström, M.; Dedinaite, A. Trapped Non-Equilibrium States in Aqueous Solutions of Oppositely Charged Polyelectrolytes and Surfactants: Effects of Mixing Protocol and Salt Concentration. *Colloids Surf., A* **2005**, *253*, 83.
- (22) Mezei, A.; Mészáros, R. Novel Method for the Estimation of the Binding Isotherms of Ionic Surfactants on Oppositely Charged Polyelectrolytes. *Langmuir* **2006**, *22*, 7148.
- (23) Mezei, A.; Ábrahám, Á.; Pojják, K.; Mészáros, R. The Impact of Electrolyte on the Aggregation of the Complexes of Hyperbranched Poly(Ethyleneimine) and Sodium Dodecyl Sulfate. *Langmuir* **2009**. <https://doi.org/10.1021/la9003388>.
- (24) Kizilay, E.; Kayitmazer, A. B.; Dubin, P. L. Complexation and Coacervation of Polyelectrolytes with Oppositely Charged Colloids. *Adv. Colloid Interface Sci.* **2011**, *167* (1–2), 24–37. <https://doi.org/10.1016/j.cis.2011.06.006>.

- (25) Pojjażk, K.; Bertalanits, E.; Mezőszáros, R. Effect of Salt on the Equilibrium and Nonequilibrium Features of Polyelectrolyte/Surfactant Association. *Langmuir* **2011**. <https://doi.org/10.1021/la2021353>.
- (26) Hoffmann, I.; Simon, M.; Farago, B.; Schweins, R.; Falus, P.; Holderer, O.; Gradzielski, M. Structure and Dynamics of Polyelectrolyte Surfactant Mixtures under Conditions of Surfactant Excess. *J. Chem. Phys.* **2016**, *145* (12), 124901. <https://doi.org/10.1063/1.4962581>.
- (27) Goswami, M.; Borreguero, J. M.; Pincus, P. A.; Sumpter, B. G. Surfactant-Mediated Polyelectrolyte Self-Assembly in a Polyelectrolyte-Surfactant Complex. *Macromolecules* **2015**. <https://doi.org/10.1021/acs.macromol.5b02145>.
- (28) Piculell, L.; Lindman, B. Association and Segregation in Aqueous Polymer/Polymer, Polymer/Surfactant, and Surfactant/Surfactant Mixtures: Similarities and Differences. *Adv. Colloid Interface Sci.* **1992**. [https://doi.org/10.1016/0001-8686\(92\)80011-L](https://doi.org/10.1016/0001-8686(92)80011-L).
- (29) Chiappisi, L.; Hoffmann, I.; Gradzielski, M. Complexes of Oppositely Charged Polyelectrolytes and Surfactants - Recent Developments in the Field of Biologically Derived Polyelectrolytes. *Soft Matter*. 2013. <https://doi.org/10.1039/c3sm27698h>.
- (30) Li, D.; Wagner, N. J. Universal Binding Behavior for Ionic Alkyl Surfactants with Oppositely Charged Polyelectrolytes. *J. Am. Chem. Soc.* **2013**. <https://doi.org/10.1021/ja408587u>.
- (31) Ábraham, Á.; Campbell, R. A.; Kardos, A.; Varga, I. Effects of Ionic Strength on the Surface Tension and Nonequilibrium Interfacial Characteristics of Poly(Sodium Styrene Sulfonate)/ Dodecyltrimethylammonium Bromide Mixtures. *Langmuir* **2014**, *30*, 4970.
- (32) Zhao, W.; Wang, Y. Coacervation with Surfactants: From Single-Chain Surfactants to Gemini Surfactants. *Advances in Colloid and Interface Science*. 2017. <https://doi.org/10.1016/j.cis.2016.04.005>.
- (33) Wang, Y.; Kimura, K.; Dubin, P. L.; Jaeger, W. Polyelectrolyte-Micelle Coacervation: Effects of Micelle Surface Charge Density, Polymer Molecular Weight, and

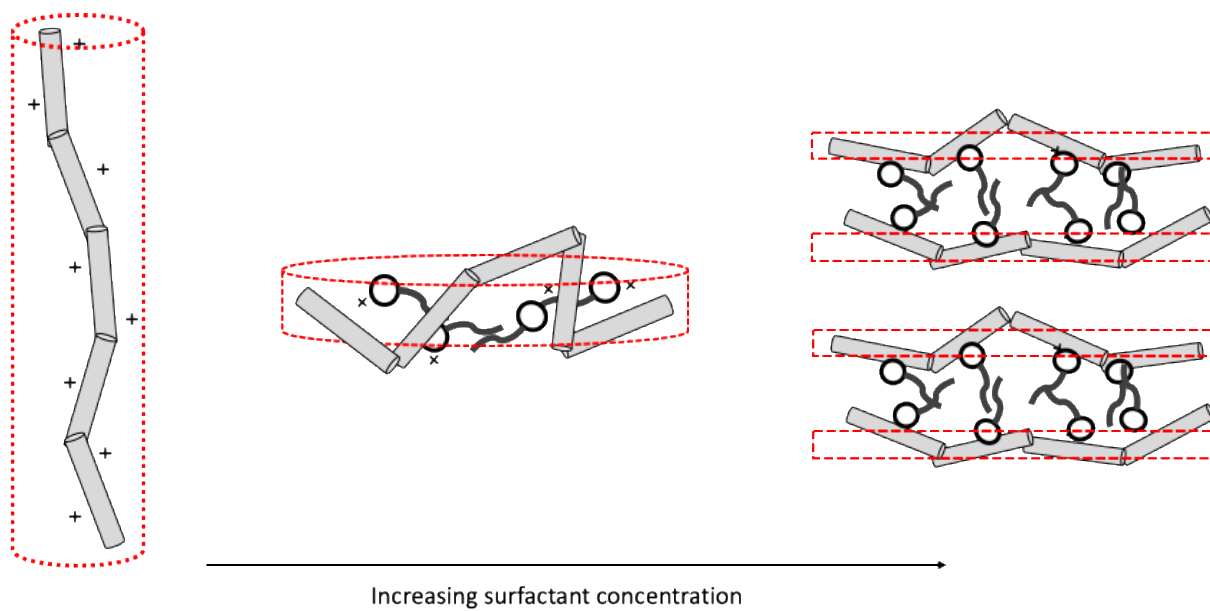
- Polymer/Surfactant Ratio. *Macromolecules* **2000**. <https://doi.org/10.1021/ma991886y>.
- (34) Stilbs, P.; Paulsen, K.; Griffiths, P. C. Global Least-Squares Analysis of Large, Correlated Spectral Data Sets: Application to Component-Resolved FT-PGSE NMR Spectroscopy. *J. Phys. Chem.* **1996**, *100* (20). <https://doi.org/10.1021/jp9535607>.
- (35) Griffiths, P. C.; Paul, A.; Stilbs, P.; Pettersson, E. Electrophoretic Nuclear Magnetic Resonance (ENMR) - A New Tool for Studying Counterion Binding in Mixed Surfactant Systems. *Langmuir* **2003**, *19* (20). <https://doi.org/10.1021/la034793p>.
- (36) Arnold, O.; Bilheux, J. C.; Borreguero, J. M.; Buts, A.; Campbell, S. I.; Chapon, L.; Doucet, M.; Draper, N.; Ferraz Leal, R.; Gigg, M. A.; Lynch, V. E.; Markvardsen, A.; Mikkelsen, D. J.; Mikkelsen, R. L.; Miller, R.; Palmen, K.; Parker, P.; Passos, G.; Perring, T. G.; Peterson, P. F.; Ren, S.; Reuter, M. A.; Savici, A. T.; Taylor, J. W.; Taylor, R. J.; Tolchenov, R.; Zhou, W.; Zikovsky, J. Mantid - Data Analysis and Visualization Package for Neutron Scattering and μ SR Experiments. *Nucl. Instruments Methods Phys. Res. Sect. A Accel. Spectrometers, Detect. Assoc. Equip.* **2014**. <https://doi.org/10.1016/j.nima.2014.07.029>.
- (37) Kříž, J.; Dybal, J.; Kurková, D. Cooperative Counterion–Polyion Interactions in Polyelectrolyte Chain Dynamics: NMR and Quantum-Chemical Study of Locally Collapsed State in Dilute Poly(N-Diallyldimethylammonium Chloride) in NaCl/D₂O Solutions. *J. Phys. Chem. A* **2002**, *106* (34), 7971–7981. <https://doi.org/10.1021/jp020282k>.
- (38) Griffiths, P. C.; Paul, A.; Hirst, N. Electrophoretic NMR Studies of Polymer and Surfactant Systems. *Chem. Soc. Rev.* **2006**, *35* (2). <https://doi.org/10.1039/b501286b>.
- (39) Tsalikis, D. G.; Alexiou, T. S.; Alatas, P. V.; Mavrantzas, V. G. Conformation and Diffusivity of Ring and Linear Polyethylene Oxide in Aqueous Solution: Molecular Topology Dependent Concentration Effects and Comparison with Experimental Data. *Macromol. Theory Simulations* **2020**, *n/a* (n/a), 2000016. <https://doi.org/10.1002/mats.202000016>.
- (40) Fegyver, E.; Mészáros, R. Complexation between Sodium Poly(Styrenesulfonate) and

- Alkyltrimethylammonium Bromides in the Presence of Dodecyl Maltoside. *J. Phys. Chem. B* **2015**. <https://doi.org/10.1021/acs.jpcc.5b01206>.
- (41) Pojják, K.; Fegyver, E.; Mészáros, R. Effect of Linear Nonionic Polymer Additives on the Kinetic Stability of Dispersions of Poly(Diallyldimethylammonium Chloride)/Sodium Dodecylsulfate Nanoparticles. *Langmuir* **2013**. <https://doi.org/10.1021/la4021542>.
- (42) Patel, L. Electrophoretic NMR Characterization of Self-Assembling Systems, University of Greenwich, 2019.
- (43) Chen, Z.; Li, X.-W.; Zhao, K.-S.; Xiao, J.-X.; Yang, L.-K. Dielectric Spectroscopy Investigation on the Interaction of Poly(Diallyldimethylammonium Chloride) with Sodium Decyl Sulfate in Aqueous Solution. *J. Phys. Chem. B* **2011**, *115* (19), 5766–5774. <https://doi.org/10.1021/jp200486u>.
- (44) Staples, E.; Tucker, I.; Penfold, J.; Warren, N.; Thomas, R. K.; Taylor, D. J. F. Organization of Polymer-Surfactant Mixtures at the Air-Water Interface: Sodium Dodecyl Sulfate and Poly(Dimethyldiallylammonium Chloride). *Langmuir* **2002**. <https://doi.org/10.1021/la020034f>.
- (45) Cooke, D. J.; Dong, C. C.; Lu, J. R.; Thomas, R. K.; Simister, E. A.; Penfold, J. Interaction between Poly(Ethylene Oxide) and Sodium Dodecyl Sulfate Studied by Neutron Reflection. *J. Phys. Chem. B* **1998**, *102* (25), 4912–4917. <https://doi.org/10.1021/jp9804291>.
- (46) Chiappisi, L.; Prévost, S.; Grillo, I.; Gradzielski, M. Chitosan/Alkylethoxy Carboxylates: A Surprising Variety of Structures. *Langmuir* **2014**, *30* (7), 1778–1787. <https://doi.org/10.1021/la404718e>.
- (47) Schillén, K.; Galantini, L.; Du, G.; Del Giudice, A.; Alfredsson, V.; Carnerup, A. M.; Pavel, N. V; Masci, G.; Nyström, B. Block Copolymers as Bile Salt Sequestrants: Intriguing Structures Formed in a Mixture of an Oppositely Charged Amphiphilic Block Copolymer and Bile Salt. *Phys. Chem. Chem. Phys.* **2019**, *21* (23), 12518–12529. <https://doi.org/10.1039/C9CP01744E>.

- (48) Merta, J.; Garamus, V. M.; Willumeit, R.; Stenius, P. Structure of Complexes Formed by PDADMAC and Sodium Palmitate. *Langmuir* **2002**. <https://doi.org/10.1021/la011867t>.
- (49) Hayter, J. B.; Penfold, J. An Analytic Structure Factor for Macroion Solutions. *Mol. Phys.* **1981**. <https://doi.org/10.1080/00268978100100091>.
- (50) Joanny, J. F.; Leibler, L. Weakly Charged Polyelectrolytes in a Poor Solvent. *J. Phys. Paris* **1990**, *51*, 545. <https://doi.org/10.1051/jphys:01990005106054500>.
- (51) Liberatore, M. W.; Wyatt, N. B.; Henry, M.; Dubin, P. L.; Foun, E. Shear-Induced Phase Separation in Polyelectrolyte/Mixed Micelle Coacervates. *Langmuir* **2009**. <https://doi.org/10.1021/la903260r>.
- (52) Basak, A.; Himadri, K.; Bohidar, B.; Mattison, K. W.; Bose, A.; Sarkar, J.; Basek, K. A.; Bose, K. W.; Kayitmazer, A. B.; Bohidar, H. B.; Hashidzume, A.; Russo, P. S.; Jaeger, W.; Dubin, P. L. Mesophase Separation and Probe Dynamics in Protein-Polyelectrolyte Coacervates Citation/Publisher Attribution Mesophase Separation and Probe Dynamics in Protein–Polyelectrolyte Coacervates {. *Soft Matter* **2007**. <https://doi.org/10.1039/b701334e>.
- (53) Kumar, A.; Dubin, P. L.; Hennon, M. J.; Li, Y.; Jaeger, W. Temperature-Dependent Phase Behavior of Polyelectrolyte-Mixed Micelle Systems. In *Journal of Physical Chemistry B*; 2007. <https://doi.org/10.1021/jp067919a>.
- (54) Comert, F.; Nguyen, D.; Rushanan, M.; Milas, P.; Xu, A. Y.; Dubin, P. L. Precipitate-Coacervate Transformation in Polyelectrolyte-Mixed Micelle Systems. *J. Phys. Chem. B* **2017**. <https://doi.org/10.1021/acs.jpcc.6b12895>.
- (55) Dubin, P. L.; Oteri, R. Association of Polyelectrolytes with Oppositely Charged Mixed Micelles. *J. Colloid Interface Sci.* **1983**. [https://doi.org/10.1016/0021-9797\(83\)90205-9](https://doi.org/10.1016/0021-9797(83)90205-9).
- (56) Comert, F.; Azarikia, F.; Dubin, P. L. Polysaccharide Zeta-Potentials and Protein-Affinity. *Phys. Chem. Chem. Phys.* **2017**. <https://doi.org/10.1039/c7cp02641b>.

- (57) Corbyn, C. P.; Fletcher, P. D. I.; Gemici, R.; Dias, R. S.; Miguel, M. G. Re-Dissolution and de-Compaction of DNA–Cationic Surfactant Complexes Using Non-Ionic Surfactants. *Phys. Chem. Chem. Phys.* **2009**, *11* (48), 11568–11576. <https://doi.org/10.1039/B916116C>.
- (58) Janiak, J.; Tomšič, M.; Lundberg, D.; Olofsson, G.; Piculell, L.; Schillén, K. Soluble Aggregates in Aqueous Solutions of Polyion–Surfactant Ion Complex Salts and a Nonionic Surfactant. *J. Phys. Chem. B* **2014**, *118* (32), 9745–9756. <https://doi.org/10.1021/jp411701g>.
- (59) Schmidt, F.; Pugliese, A.; Santini, C. C.; Castiglione, F.; Schönhoff, M. Spectral Deconvolution in Electrophoretic NMR to Investigate the Migration of Neutral Molecules in Electrolytes. *Magn. Reson. Chem.* **2020**, *58* (3), 271–279. <https://doi.org/10.1002/mrc.4978>.

Graphical Abstract



The binding of anionic sodium dodecylsulphate to a low molecular weight sample of poly(diallyldimethylammonium chloride) leads to surfactant-templated collapse of the rod-like polyelectrolyte solution conformation forming disc-like and lamellar structures coincident with the macroscopic phase boundary.